INTERNATIONAL JOURNAL FOR NUMERICAL METHODS IN FLUIDS, VOL. 4, 247–269 (1984)

A FINITE ELEMENT METHOD TO SOLVE THE NAVIER–STOKES EQUATIONS USING THE METHOD OF CHARACTERISTICS

J. P. HUFFENUS AND D. KHALETZKY

NEYRPIC Company BP 75, 38041 Grenoble Cédex, France

SUMMARY

We present a simple and efficient finite element method to solve the Navier–Stokes equations in primitive variables V, p. It uses (a) an explicit advection step, by upwind differencing. Improvement with regard to the classical upwind differencing scheme of the first order is realized by accurate calculation of the characteristic curve across several elements, and higher order interpolation; (b) an implicit diffusion step, avoiding any theoretical limitation on the time increment, and (c) determination of the pressure field by solving the Poisson equation. Two laminar flow calculations are presented and compared to available numerical and experimental results.

KEY WORDS Finite Elements Navier–Stokes Driven Cavity Flow Past a Cylinder

1. INTRODUCTION

In a previous paper[1] we have pointed out the interest of using the method of characteristics to solve the transport equation:

$$\frac{\partial F}{\partial t} + u\frac{\partial F}{\partial x} = 0 \tag{1}$$

where u is a given velocity field, and $F(x, t)$ a scalar function. Figure 1 recalls our notations.

When integrated over a time step, equation (1), written at location i, becomes:

$$F_i^{n+1} = F^* \tag{2}$$

The solution of (2) then requires the interpolation of the value F^* from the values at neighbouring nodes.

In a multidimensional calculation with a non-constant velocity field, F^* must be located in the domain, i.e. the characteristic curve must be integrated between times $n+1$ and n, before performing the interpolation.

Recent papers, and in particular Reference 2, advocate the same method to solve the advection problem. However, advection is not the sole problem in the Navier–Stokes equations. The velocity–pressure coupling, or Stokes problem, is also difficult, especially with F.E. methods. Several 'F.E. Stokes solvers' are available in the literature. Our method is directly derived from old F.D. methods in primitive variables V, p.[1,3,4]

0271–2091/84/030247–23$02.30

Received 13 July 1982
Revised 20 November 1982

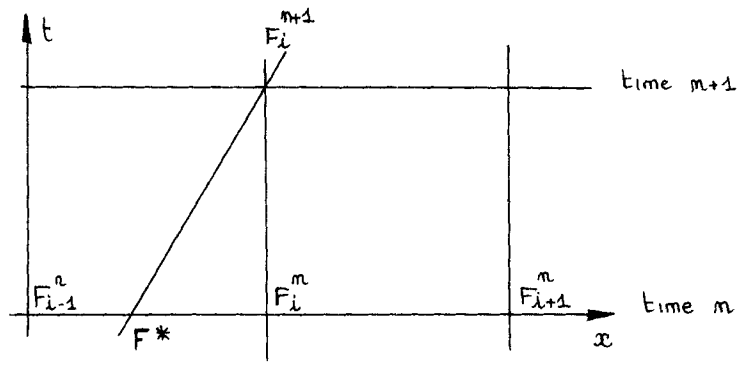

Figure 1. Method of characteristics

2. THE METHOD OF CHARACTERISTICS IN AN F.E. CONTEXT

Since all the nodal values are known at time n, the components of the velocity, and the transported function F, are piecewise analytic, owing to the shape function of each element. This feature allows us to compute the characteristic curve, and then to interpolate the value F^*. The calculation of the characteristic curve consists in solving the differential equation:

$$\frac{dM}{dt} = V(M, t)$$

from time $n+1$, to time n. When only a steady state flow or a slow transient flow is considered, V can be assumed to be independent of time, between times n and $n+1$. Then we only solve:

$$\frac{dM}{dt} = V(M) \tag{3}$$

Several methods are envisaged to solve this equation.

2.1. *The rectilinear characteristic*

V is assumed to be locally constant and:

$$M^* = M_i^{n+1} - V\,\delta t$$

where M^* is the location of F^*, M_i^{n+1} the location of node i, δt the time increment. To achieve the advection step, we determine the element which contains M^*, and compute the value F^*, using the shape function of this element.

2.2. *The curvilinear characteristic*

In this case, equation (3) is integrated more carefully, using one step of the Runge–Kutta algorithm per crossed element. With the RK1 method (Runge–Kutta of first order), the characteristic curve is rectilinear on each crossed element. With a moderate time increment δt, it is not very different from the previous one. When RK2 or RK4 methods are used, the characteristic curve is curvilinear inside each crossed element. While integrating equation (3), the crossed element is always known. Hence, when this calculation is terminated, the

element which contains M^* is already determined, and the advection step can be achieved by interpolating the value F^*.

3. FORMULATION IN V^* OF THE NAVIER–STOKES EQUATIONS

The Navier–Stokes equations can be written in the following form:

$$\text{momentum} \quad \frac{DV}{Dt} = -\nabla p + \nu \nabla^2 V \tag{4}$$

$$\text{continuity} \quad \nabla V = 0 \tag{5}$$

Let us integrate the equations (4) over a time step. Using the notations defined in the introduction, we introduce the scalar quantities u^* and v^* (in two dimensions). These values are the components of the vector V^*. Then the advection term of (4) becomes:

$$\frac{DV}{Dt} = \frac{V^{n+1} - V^*}{\delta t}$$

where δt is the time increment.

In order to obtain a workable scheme, the right-hand side of equation (4) must be averaged over the time step. We choose a fully implicit evaluation:

$$\frac{1}{\delta t} \oint_t^{t+\delta t} (-\nabla p + \nu \nabla^2 V)\, dt \simeq -\nabla p^{n+1} + \nu \nabla^2 V^{n+1}$$

Thus the system (4), (5) becomes:

$$\frac{V^{n+1} - V^*}{\delta t} = -\nabla p^{n+1} + \nu \nabla^2 V^{n+1} \tag{6}$$

$$\nabla V^{n+1} = 0 \tag{7}$$

The system of coupled equations (6), (7) can then be transformed into a set of uncoupled elliptical problems, by taking the divergence of (6) and using the condition (7):

$$\nabla^2 p = \nabla V^* / \delta t \tag{8}$$

Let us summarize then the calculation needed to carry the solution forwards, from time n, to time $n+1$:

(i) Apply the method of the characteristics, to determine u^* and v^* at each node.

(ii) Solve the problem (8) usually with Neumann boundary conditions.

(iii) Solve the equations (6), usually with Dirichlet boundary conditions.

Equation (8) appears in several F.D. methods.[1,3] Roache[4] summarizes several references where the velocity–pressure coupling is solved in this way. The method of characteristics provides an easy formulation of the second member of (8). It can be noted that since:

$$V^* = V^n - \delta t (V . \nabla V)^n$$

the divergence term div V^* implicitly contains the necessary stabilizing term $\nabla V^n / \delta t$. The mathematical properties of this formulation were widely studied in an F.D. context. Its main drawback is that some Neumann boundary conditions must be inferred from the velocity field, in order to solve (8).

For instance, the pressure gradient along a no-slip wall can be written as:

$$\nabla p . n = -\partial \tau / \partial s$$

where s and n are respectively the tangential and normal directions to the wall, τ the shear stress $\tau = \nu\, \partial u_s/\partial n$.

When an inlet velocity profile $u_n(s)$ is specified:

$$\nabla p \,.\, n = \nu\, \partial u_n/\partial s$$

4. FINITE ELEMENT METHOD

4.1. *Basic principle*

In a finite element context, the previously described algorithm remains simple:

(a) as stated in Section 2, the interpolation of values V^* can be easily done by using the shape function of the element containing M^*

(b) the second order differential problems appearing in second and third steps, are perfectly suited to a finite element method.

By application of the principle of virtual power,[5] we obtain the following variational statement, which corresponds to the set of equations (8), (6) for the two-dimensional case:

$$\int_{\mathscr{D}} \nabla^2 p\, \delta p \, \mathrm{d}\omega = \frac{1}{\delta t} \int_{\mathscr{D}} \nabla V^* \, \delta p \, \mathrm{d}\omega \tag{9}$$

$$\int_{\mathscr{D}} \left(\frac{1}{\delta t} u - \nu \nabla^2 u\right) \delta u \, \mathrm{d}\omega = \int_{\mathscr{D}} -\frac{\partial p}{\partial x} \delta u \, \mathrm{d}\omega + \frac{1}{\delta t} \int_{\mathscr{D}} u^* \, \delta u \, \mathrm{d}\omega \tag{10}$$

$$\int_{\mathscr{D}} \left(\frac{1}{\delta t} v - \nu \nabla^2 v\right) \delta v \, \mathrm{d}\omega = \int_{\mathscr{D}} -\frac{\partial p}{\partial y} \delta v \, \mathrm{d}\omega + \frac{1}{\delta t} \int_{\mathscr{D}} v^* \, \delta v \, \mathrm{d}\omega \tag{11}$$

$\int_{\mathscr{D}} f \, \mathrm{d}\omega$ is the surface integral of a function f over the computational field $\mathscr{D}$. Let Γ be the boundary of $\mathscr{D}$. After integration by parts of the equations, the weak formulation follows. Let $n = (\sin\theta, -\cos\theta)$ be the normal vector to the contour Γ.

$$\int_{\mathscr{D}} \nabla p \,.\, \nabla\, \delta p \, \mathrm{d}\omega = -\frac{1}{\delta t} \int_{\mathscr{D}} \delta p\, \nabla V^* \, \mathrm{d}\omega + \oint_{\Gamma} \delta p\, \nabla p \,.\, n \, \mathrm{d}s \tag{12}$$

$$\int_{\mathscr{D}} \left(\frac{1}{\delta t} u\, \delta u + \nu\, \nabla u\, \nabla\, \delta u\right) \mathrm{d}\omega = \frac{1}{\delta t} \int_{\mathscr{D}} u^* \, \delta u \, \mathrm{d}\omega + \int_{\mathscr{D}} p \frac{\partial\, \delta u}{\partial x} \mathrm{d}\omega + \oint_{\Gamma} (\nu\, \nabla u \,.\, n - p \sin\theta)\, \delta u \, \mathrm{d}s \tag{13}$$

$$\int_{\mathscr{D}} \left(\frac{1}{\delta t} v\, \delta v + \nu\, \nabla v\, \nabla\, \delta v\right) \mathrm{d}\omega = \frac{1}{\delta t} \int_{\mathscr{D}} v^* \, \delta v \, \mathrm{d}\omega + \int_{\mathscr{D}} p \frac{\partial\, \delta u}{\partial y} \mathrm{d}\omega + \oint_{\Gamma} (\nu\, \nabla v \,.\, n + p \cos\theta)\, \delta v \, \mathrm{d}s \tag{14}$$

Consider now a triangulation of the domain. On each triangle,

$$u = \phi^{\mathrm{T}} u^n, \qquad v = \phi^{\mathrm{T}} v^n, \qquad p = \varphi^{\mathrm{T}} p^n \tag{15}$$

ϕ and φ are the shape functions for the velocity and pressure fields respectively, u^n, v^n, p^n are the column vectors of the nodal values.

Substituting (15) into (12) we obtain the following expression for arbitrary variations of δp and interior element A:

$$k p^n = -\frac{1}{\delta t} (C_x u^{*n} + C_y v^{*n}) \tag{16}$$

for variations of δu:

$$\left(\frac{1}{\delta t} M + \nu K\right) u^n = \frac{1}{\delta t} M u^{*n} + C_x^{\mathrm{T}} p^n \tag{17}$$

for variations of δv:

$$\left(\frac{1}{\delta t} M + \nu K\right) v^n = \frac{1}{\delta t} M v^{*n} + C_y^{\mathrm{T}} p^n$$

where

$$k = \int_A (\dot{\varphi}_x \dot{\varphi}_x^{\mathrm{T}} + \dot{\varphi}_y \dot{\varphi}_y^{\mathrm{T}})\, \mathrm{d}\omega, \qquad K = \int_A (\dot{\phi}_x \dot{\phi}_x^{\mathrm{T}} + \dot{\phi}_y \dot{\phi}_y^{\mathrm{T}})\, \mathrm{d}\omega$$

$$C_x = \int_A \varphi \dot{\phi}_x^{\mathrm{T}}\, \mathrm{d}\omega, \qquad C_y = \int_A \varphi \dot{\phi}_y^{\mathrm{T}}\, \mathrm{d}\omega$$

$$M = \int_A \phi \phi^{\mathrm{T}}\, \mathrm{d}\omega$$

After assembling and applying the boundary conditions (as an example pressure gradients for (12), and imposed velocity profiles for (13), (14)) we obtain 3 positive definite matrices which lead to the 3 linear systems to be solved in order to reach the state $n+1$.

4.2. Choice of the shape function

The simplest choice is of course the linear shape function for φ and ϕ:

$$\varphi^{\mathrm{T}} = \phi^{\mathrm{T}} = \{l_1, l_2, l_3\} \tag{18}$$

where l_1, l_2, l_3 are the area co-ordinates of the triangle.

This method was implemented by the authors, and tested on several flow calculations. As expected from the linear interpolation of the value V^*, numerical damping was important. Moreover, we have found an unstable behaviour of the solution in some cases like the flow behind a sudden widening, or in the wake of an obstacle. For these reasons, this method has been given up.

A better choice is used by Glowinsky *et al.*,[6] in a different method. It is the P_1–P_2 triangle or Taylor–Hood element: parabolic six-node triangles for the velocities, linear three-node triangles for the pressure (Figure 2).

In that case,

$$\begin{aligned} \varphi &= \{l_1, l_2, l_3\} \\ \phi &= \{l_1(2l_1-1), l_2(2l_2-1), l_3(2l_3-1), 4l_1l_2, 4l_2l_3, 4l_1l_3\} \end{aligned} \tag{19}$$

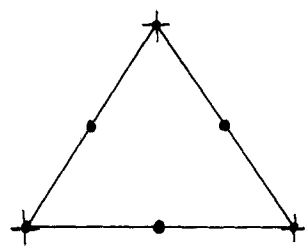

Figure 2. The P_1–P_2 element: ● velocities, + pressure

This method will be called later in the text PEFE2 (Poisson equation and finite elements of 2nd order).

4.3. *Boundary conditions*

Boundary conditions for velocity components are in general easy, which is one of the main advantages of the V, p formulation. For an inlet condition, and a no slip wall, values of u and v are simply specified. For a horizontal (resp. vertical) symmetry axis, we specify $v = 0$ and $\partial u/\partial y = 0$ (resp. $u = 0$ and $\partial v/\partial x = 0$). For a vertical (resp. horizontal) outlet boundary we can use $p = 0$ as a normal boundary condition, and $v = 0$ (resp. $u = 0$) as a tangential boundary condition. Another possibility for an outlet condition is to specify $V = V^* Q_I/Q_O$ where Q_I is the discharge at the inlet and Q_O the discharge at outlet.

To solve equation (8), and except for the boundary where $p = 0$, expressions for the pressure gradient can be derived from the momentum equation (see Section 3). The approximation of zero pressure gradient can also be used. We have run several calculations with both formulations, and in particular the examples presented herein. We always found that the exact formulation of the pressure gradient did not bring any significant improvement with regard to the zero pressure gradient approximation. Consequently, we believe that for a wide range of practical applications, the zero pressure gradient is workable.

Before concluding the presentation of the PEFE2 method, it is of interest to make some comments about the incompressibility condition. This condition is not ensured for each element separately, as could be done with a penalization method. However, the global solution is very acceptably conservative, as will be seen later, when considering the results for the driven cavity flow. This good feature also appears in problems with an inlet and an outlet. In that case, the discrepancy between the inlet and outlet discharges never exceeds 1 or 2 per cent, when the condition $p = 0$ is specified at the outlet. When setting $V = V^* Q_I/Q_O$, the error $\varepsilon = |1 - Q_I/Q_O|$ seldom exceeds 1 per mille, except at the beginning of a calculation, when starting from a non-conservative velocity field.

4.4. *Other possible methods*

As stated in the introduction, the treatment of advection by the method of characteristics can be associated with any solver of the Stokes problem, to solve the Navier–Stokes equations.

Let us review some recent F.E. methods[2,6,7,8] to solve the following Stokes problem, restricting ourselves to the Taylor–Hood element.

$$\begin{cases} \alpha V - \nabla^2 V = -\nabla p + S & (20) \\ \nabla V = 0 & (21) \\ V_{|\Gamma} = V_0 & (22) \end{cases}$$

where α is a scalar constant, S a given vector. V and p are the unknown velocity and pressure fields. Equation (22) represents the boundary conditions.

4.4.1. *Coupled discretization (SPFE).* The set of equations (20), (21) may also be solved by assembling and solving a single large linear system.[7,9,10] For each interior triangle the variational principle applied to the set (20), (21) leads to the system.

$$\begin{bmatrix} \alpha M + K & 0 & C_x^T \\ 0 & \alpha M + K & C_y^T \\ C_x & C_y & 0 \end{bmatrix} \begin{bmatrix} u^n \\ v^n \\ p^n \end{bmatrix} = \begin{bmatrix} S_x \\ S_y \\ 0 \end{bmatrix} \quad (23)$$

The matrices C_x, C_y are not exactly those defined in Section 4.1, since the formulation of the first order derivatives is different. In particular the integration of the continuity equation leads to:

$$\int_{\mathscr{D}} \nabla V \, \delta p \, d\omega = \int_{\Gamma} \delta p V . n \, ds - \int_{\mathscr{D}} V . \delta p \, d\omega$$

Hence:

$$C_x = \int_A \phi \dot{\phi}_x \, d\omega, \qquad C_y = \int_A \phi \dot{\phi}_y \, d\omega$$

It is generally convenient to regularize the matrix in the left-hand side of (23) by replacing the zeros on the diagonal by a small positive quantity ε. In that way the method is to some extent analogous to a penalization method, in which:

$$\nabla V + p\varepsilon = 0$$

After assembling, the overall matrix is symmetric, but very large and not positive definite. However, for a moderate number of nodes, its conditioning remains satisfactory, and the system can even be solved by a direct Gauss method, as done in our program. In the following text, we shall refer to this method by the name SPFE (Stokes problem by finite elements). In two-dimensional calculations with a moderate number of nodes ($\simeq 500$) the CPU time consumption is similar to the time with the PEFE2 method, though the storage requirement is more important. With a more important grid, and in particular in a three dimensional calculation, the direct Gauss method would become unacceptable and an efficient iterative method should be found. An extension of the conjugate gradient method with preconditioning[7] might be envisaged.

4.4.2. *Method of the trace of pressure.*[6,9] This is the method used by Benque *et al.*[2] In this method, the coupled system (20), (21) is separated into a cascade of Dirichlet problems, i.e. elliptical differential problems with Dirichlet boundary conditions. In two dimensions, this method requires 7 Dirichlet problems and the solution of an additional linear system for which the matrix A_h is full, symmetric, positive semi-definite. The size of this system is the number of pressure nodes located on the boundary Γ of the domain. When inserted in a full Navier–Stokes program, 8 calculations are required at each time step. By comparison, the PEFE2 method requires two Dirichlet problems and a smaller elliptical problem with Neumann boundary conditions.

4.4.3. *Further methods.* The penalization methods do not work well with the P_1–P_2 element, and more generally with triangles, according to Sani *et al.*[11] Results are better with quadrangles, as for instance the Q_2–Q_1 discontinuous element (8-node parabolic velocity, 4 node linear discontinuous pressures). When associated with the method of characteristics, this method can probably produce good results, but this was not the experience of the authors.

5. NUMERICAL TESTS ON THE DRIVEN CAVITY FLOW

In order to illustrate the features of our F.E. method, we calculate the square wall driven cavity flow at $Re = 1000$ (Figure 3). This is not a very good test since:

(a) Non-physical conditions must be assumed at the edges of the moving wall.

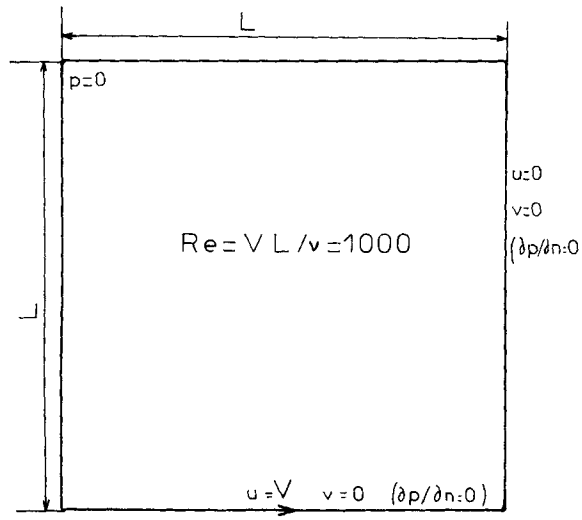

Figure 3. Driven cavity—geometry

(b) No experimental data are available (probably in relation with the non physical condition above).
(c) At high Reynolds number, the solution becomes very sensitive to the grid.
(d) The most interesting feature of an F.E. method, namely its ability to describe complex geometries, is not exhibited.

However, since a large amount of literature is available, this example is helpful to compare the results of different authors.

To perform the following calculations, we have chosen the same grid as Ibler,[8] (Figure 4). Our reference solution is the paper of Fortin *et al.*,[12] whose solution was obtained with a high order F.D. method, and a regular 40×40 grid. Several other references have been given by Thomasset.[7]

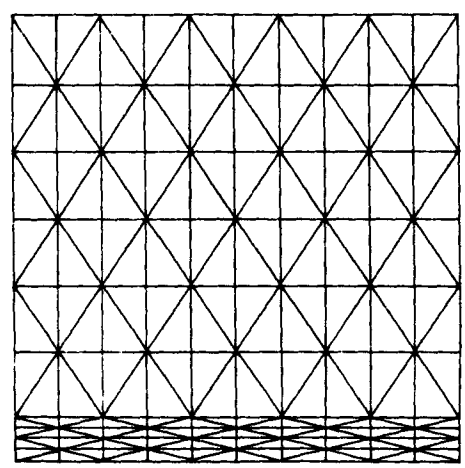

Figure 4. Driven cavity—mesh system

Table I. Summary of the results for the driven cavity

Method	MEM	CPU	Ψ_{max}	X	Y	U_{min}	Y_m	Y_0	iso Ψ	iso P
Fortin			0·085	0·55	0·42	−0·245	0·81	0·415	—	—
PEFE2 RK1	588	1·02	0·0887	0·55	0·42	−0·252	0·75	0·44	7	8
PEFE2 RK2	588	1·20	0·0829	0·54	0·42	−0·243	0·80	0·44	9	10
PEFE2 RK4	588	1·51	0·0827	0·54	0·42	−0·242	0·80	0·44	11	12
SPFE RK2	1028	1·65	0·0838	0·55	0·42	−0·248	0·80	0·432	13	14

MEM: storage requirement on an ITEL AS7, in KBytes of 8 Bits
CPU: in seconds, for one time step
Ψ_{max}, X, Y: discharge of the main vortex, and location of the eye
U_{min}: minimum velocity $U(0·5, Y_m)$ on the plotted velocity profile
Y_0: ordinate of null velocity $U(0·5, Y_0) = 0$
iso Ψ: figure number for streamlines
iso P: figure number for pressure field

For each calculation, we display:

(i) the velocity profile $u(0·5, y)$, $0 \leq y \leq 1$,
(ii) the streamlines
(iii) the pressure field.

The time increment is always $\delta t = 0·1$, thus corresponding to an F.D. Courant number $c = U\,\delta t/\delta x = 2$. Table I summarizes some scalar values corresponding to each solution.

After a short general remark we shall focus the discussion on the two main difficulties of the numerical solution of the Navier–Stokes equations, namely the treatment of advection, and the solution of the pressure–velocity coupling, or Stokes problem.

5.1. *General remarks*

All the solutions are very acceptable, with regard to the reference solution. The main characteristics of the solution are in good agreement with the reference, and in particular the values U_{min}, Y_m, Y_0 (see Table I) which are sensitive to the diffusion—physical and numerical.

5.2. *Treatment of advection* (Figure 5)

The increase of the order of the RK method from 1 to 2 improves the solution, even for a moderate time increment. For larger time steps, the curvilinear characteristic would become really necessary. On the other hand, the RK4 method brings the same results as the RK2 one, with an increase of CPU consumption. This would indicate that the characteristic of second order is accurate enough.

5.3. *Solution of the Stokes problem*

Since Ibler[8] uses the RK2 characteristic, and has done the same calculation with the same grid and time increment, we can compare efficiently three different methods to solve the Stokes problem:

(i) the trace of pressure
(ii) the coupled discretization, or SPFE
(iii) the solution of the Poisson equation, or PEFE2.

The corresponding velocity profiles are plotted in Figure 6. At ordinate $y = 0·72$, we note an inversion of curvature in the reference solution, the Ibler's solution, and not in our solutions.

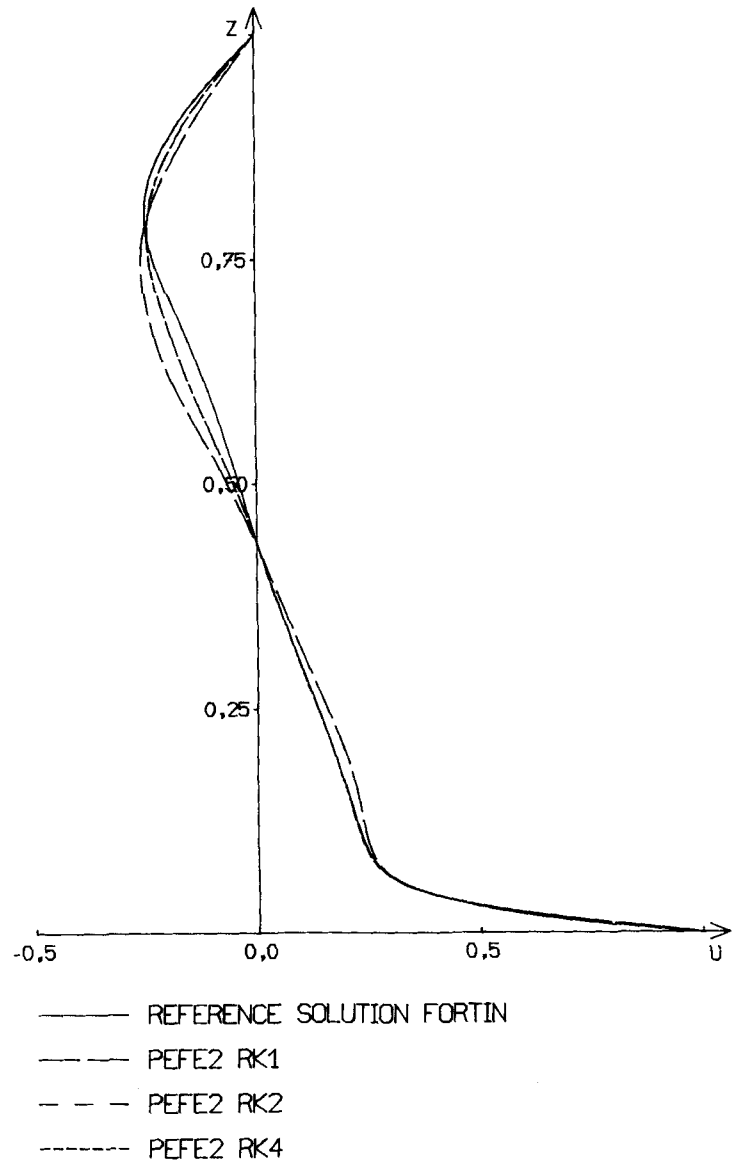

Figure 5. Velocity profile. Influence of the order of the characteristic

This difference cannot be explained up to now. Nevertheless, the four solutions are very close, which indicate that any of the quoted Stokes solvers gives interesting results, when associated with the advective term treatment by the method of the RK2 characteristic.

6. SYMMETRICAL FLOW PAST A CYLINDER

A further example of calculation is the flow past a circular cylinder at $Re = 40$, which is the maximum value for which the wake is stable. This case has the drawback of involving a very

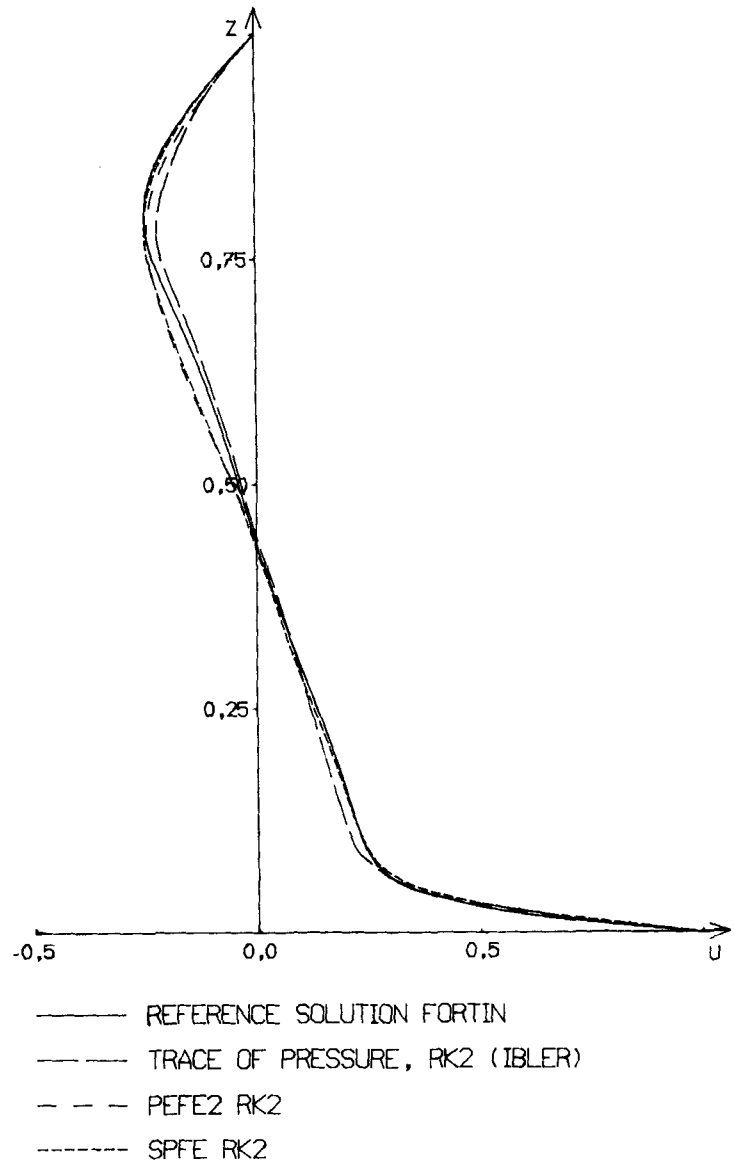

Figure 6. Velocity profile. Influence of the Stokes solver

low value of the Reynolds number, but it is interesting for several reasons:

(a) relative complexity of the geometry
(b) boundary layer with strong pressure gradient
(c) several experimental and numerical results available.

Whereas the preceding section was devoted to the comparison of different numerical methods, we now restrict ourselves to the PEFE2–RK2 method, which is obviously the simplest and cheapest method.

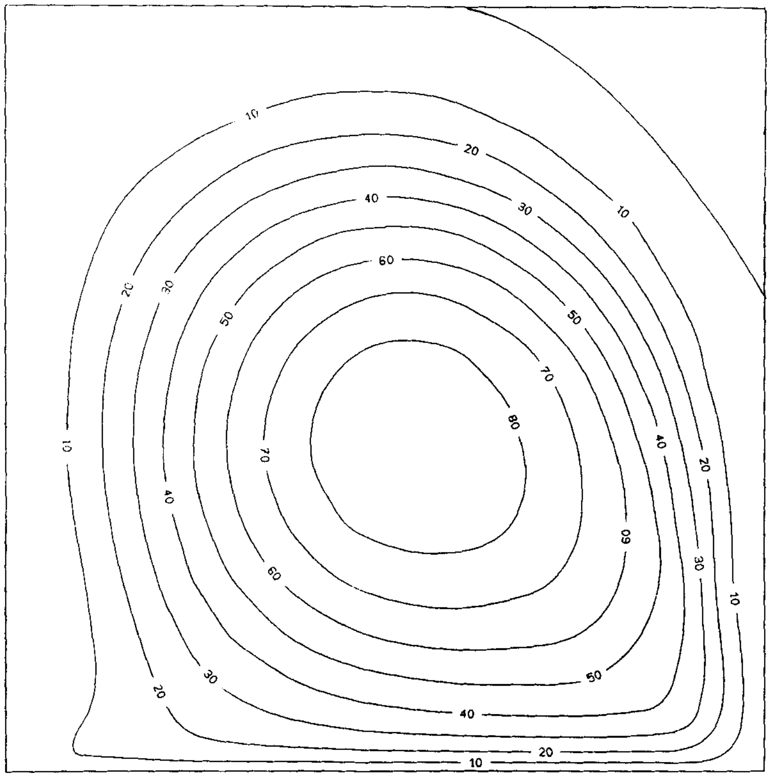

Figure 7. Streamlines, PEFE2 method, RK1 characteristic

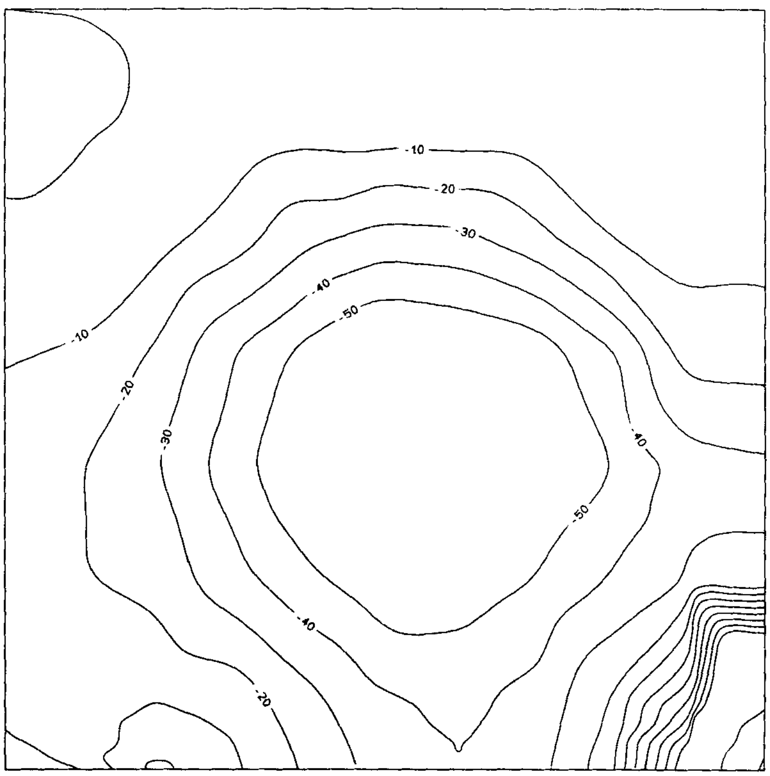

Figure 8. Pressure field, PEFE2 method, RK1 characteristic

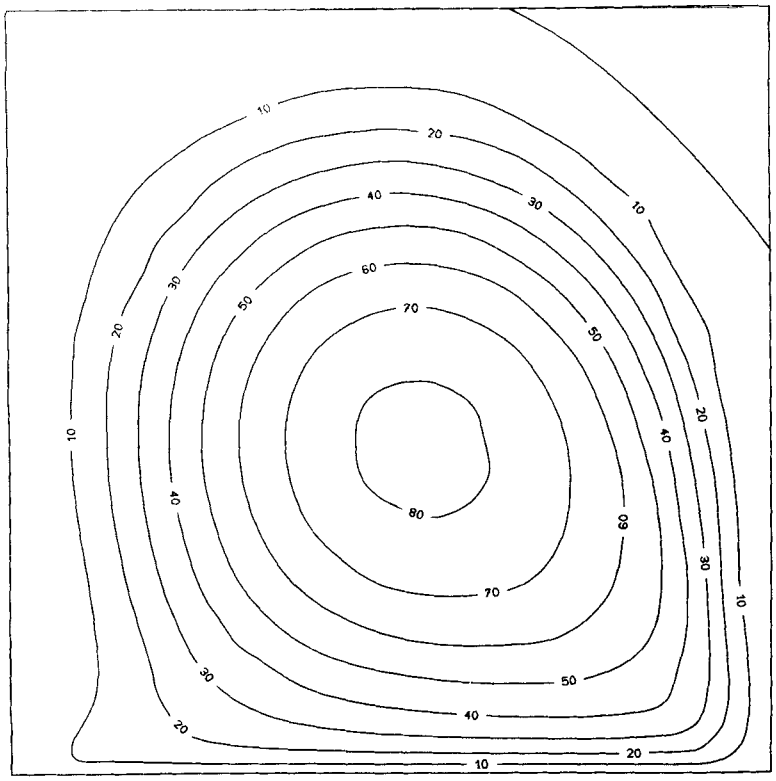

Figure 9. Streamlines, PEFE2 method, RK2 characteristic

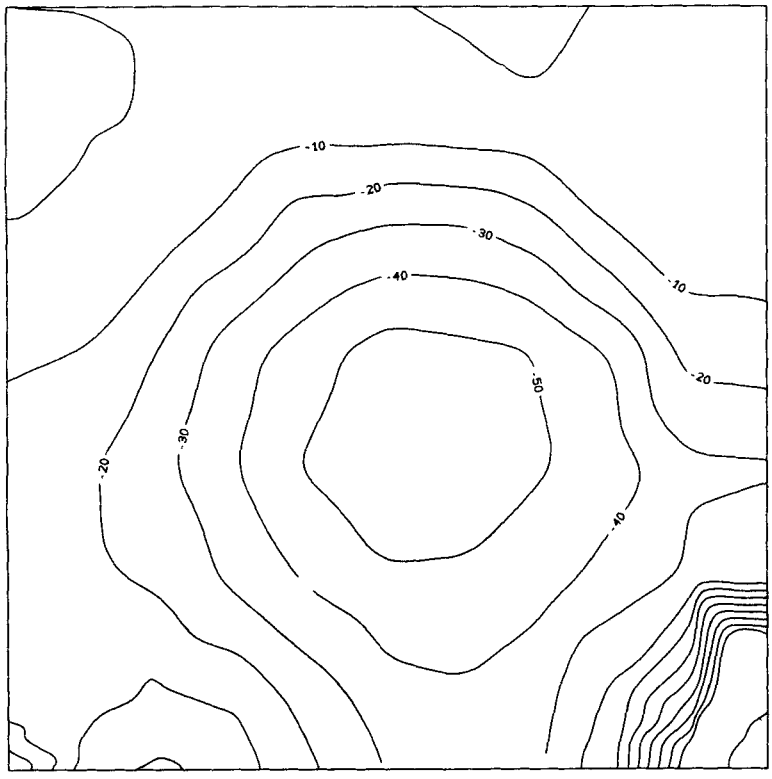

Figure 10. Pressure field, PEFE2 method, RK2 characteristic

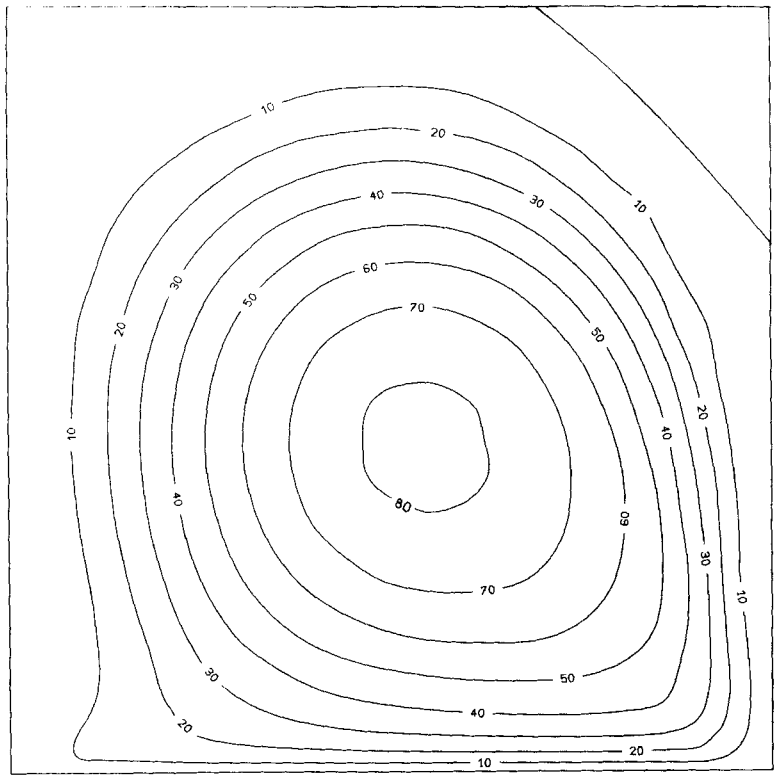

Figure 11. Streamlines, PEFE2 method, RK4 characteristic

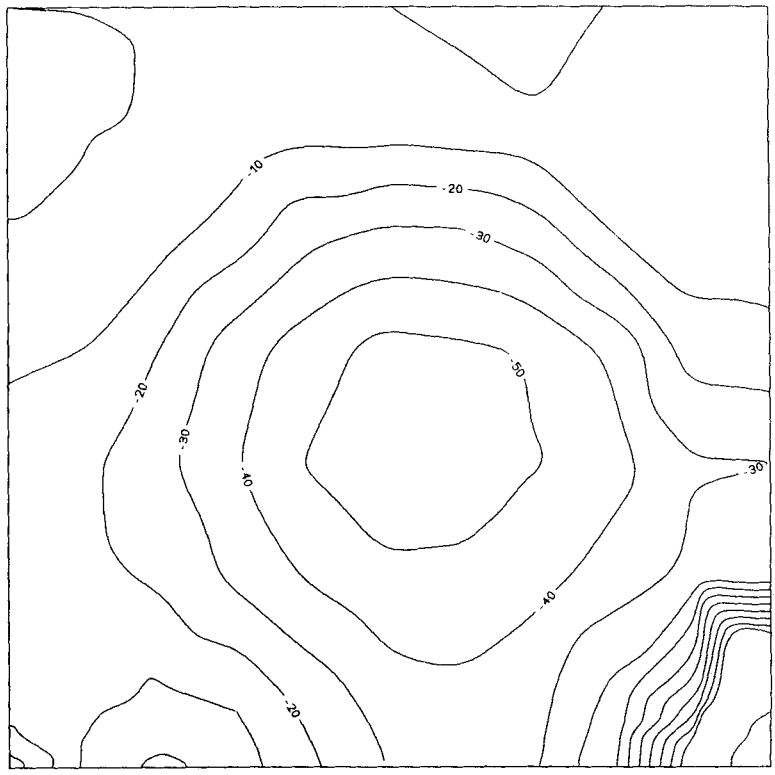

Figure 12. Pressure field, PEFE2 method, RK4 characteristic

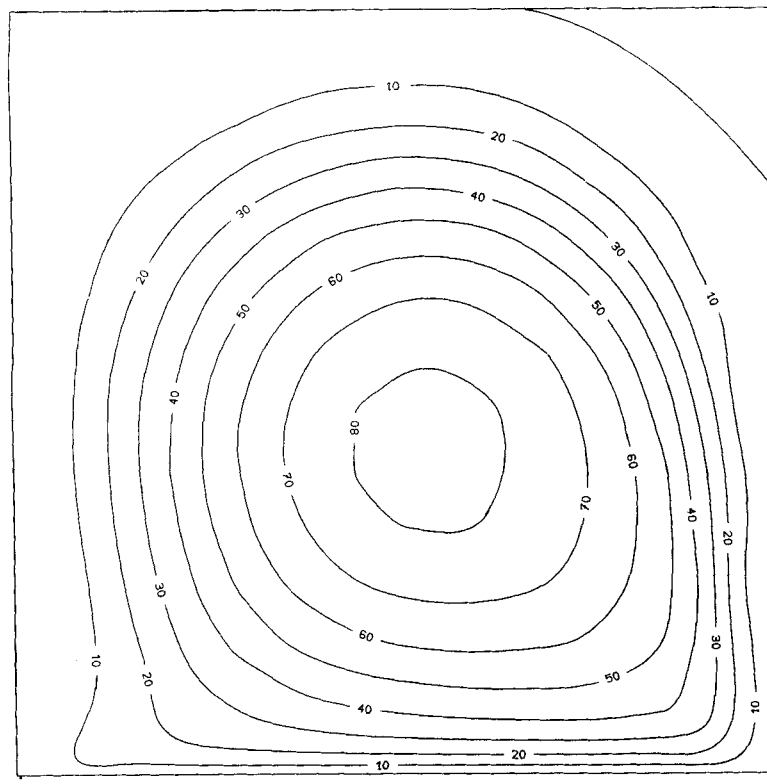

Figure 13. Streamlines, SPFE method, RK2 characteristic

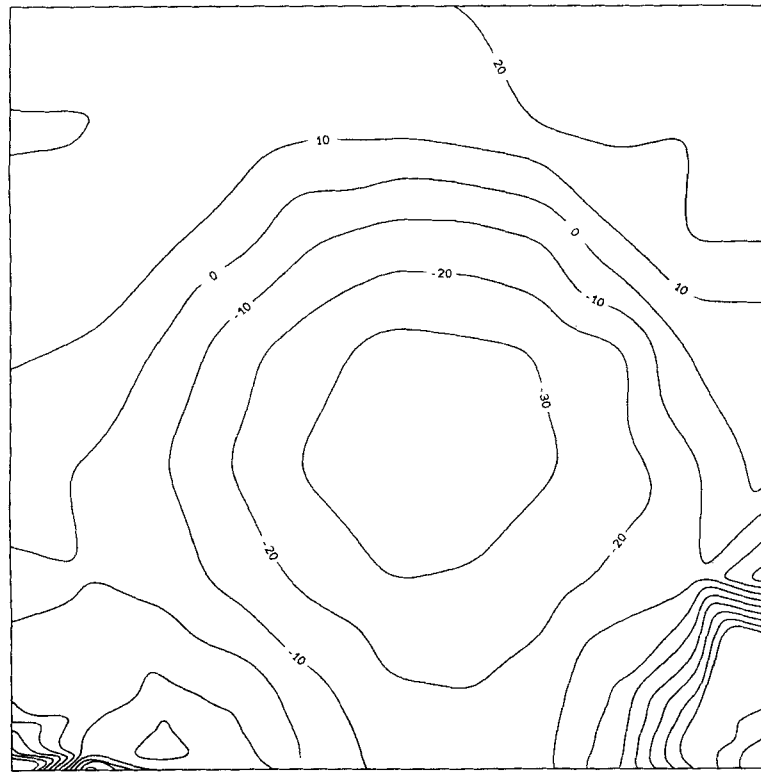

Figure 14. Pressure field, SPFE method, RK2 characteristic

6.1. *Domain of calculation and boundary conditions*

Figure 15 shows the grid used for this problem. The radius of the cylinder is $R = 1$, the height of the domain is 15, which leads to a confinement ratio of $\lambda = 1/15$. The boundary conditions are also indicated in this figure. To solve the Poisson equation, we set $\partial p/\partial n = 0$ everywhere, except at the outlet boundary where $p = 0$. Since the Reynolds number is $Re = 2R/\nu = 40$, the calculations are done with $\nu = 0{\cdot}05$.

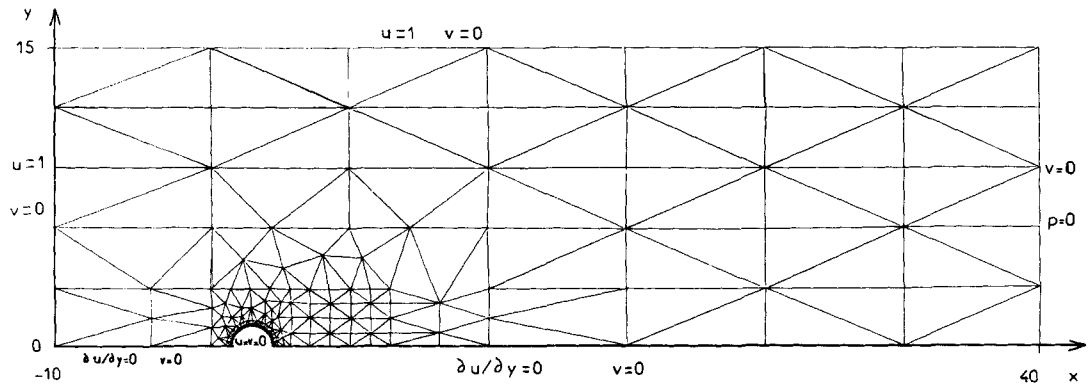

Figure 15. Flow past a cylinder—geometry

6.2. *Presentation of the results*

Each result is illustrated by plotting the shearing stress and the reduced pressure around the cylinder, and the x component of the velocity on the x axis, behind the cylinder. The shearing stress $\tau(\theta) = \nu\, \partial U_s/\partial n$ is obtained at the boundary nodes, by calculation of the partial derivatives $\partial u/\partial x$, $\partial u/\partial y$, $\partial v/\partial x$, $\partial v/\partial y$, from the velocity field.

The reduced pressure is defined as:

$$\hat{p}(\theta) = (p - p_0)/\tfrac{1}{2}\rho U_0^2$$

with $U_0 = 1$ and $\rho = 1$

p_0 is the pressure at the less perturbed point of the inlet boundary, namely the upper left corner of the domain of calculation. τ and p are also integrated around the cylinder, to evaluate the viscosity and pressure drags.

$$C_\nu = 2\int_0^\pi \tau \sin\theta \, d\theta$$

$$C_p = 2\int_0^\pi p \cos\theta \, d\theta$$

The total drag is defined by:

$$C_D = C_\nu + C_p$$

Owing to the curvilinear characteristic, and the implicit treatment of diffusive terms in the momentum equations, our method is stable without limitation on the time increment. Five calculations are done with time increments δt of 0·5, 0·2, 0·1, 0·05, 0·01. Figures 16, 17, 18 show the distribution of τ, p and u, for these 5 calculations. Furthermore, Table II summarizes the values of pressure drag C_p, viscosity drag C_ν, and total drag C_D.

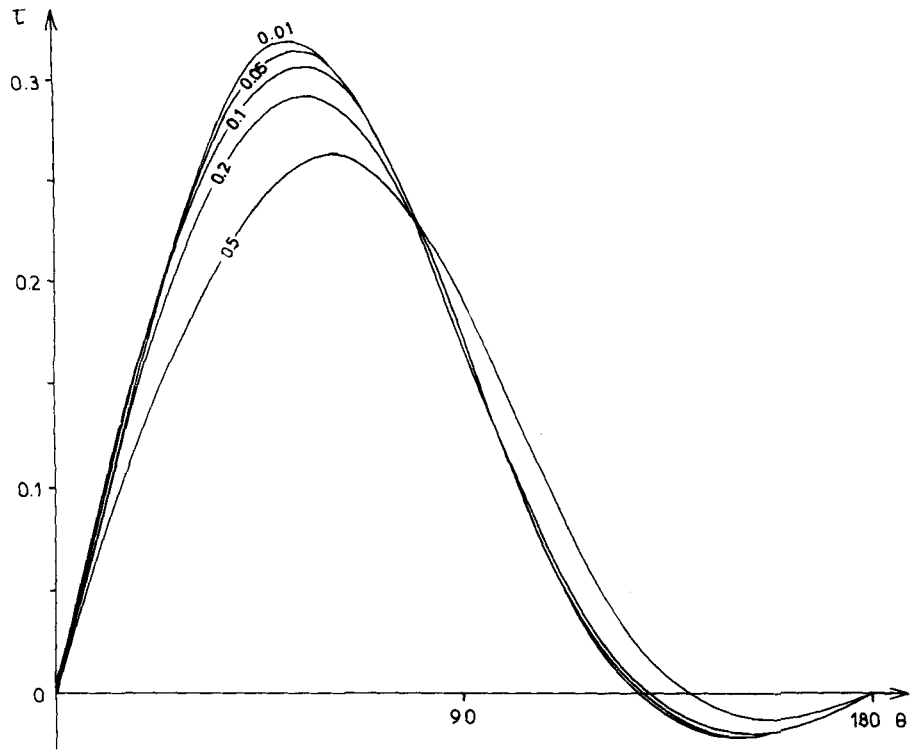

Figure 16. Shearing stress—influence of the time increment

6.3. *Influence of the time increment*

Owing to the unconditional stability of the method, a large time increment can be used in steady state calculations. This leads to important CPU time savings. The present solution for $t = 0{\cdot}5$ was reached in 100 time steps, whereas about 1000 steps were needed for $t = 0{\cdot}05$.

However, an unfortunate sensitivity of the solution to the time increment appears on these results. The poor result obtained with $\delta t = 0{\cdot}5$ is understandable, since in that case, the curvilinear characteristic crosses several triangles.

The derivatives of the velocity field not being continuous between two elements, a loss of precision in the integration of the equation (3) occurs. Moreover the assumption of Section 3:

$$\frac{1}{\delta t}\oint_t^{t+\delta t}(-\nabla p + \nu\,\nabla^2 V)\,\mathrm{d}t \simeq -\nabla p^{n+1} + \nu\,\nabla^2 V^{n+1}$$

is no longer acceptable when the starting point for the integration M^* is too far from the terminal point M^{n+1}.

However we could expect a better stabilization of the solution when $\delta t \to 0$. An explanation of this disappointing behaviour may be found in the very principle of the method of characteristics. An Eulerian treatment of advection states:

$$\frac{\mathrm{D}V}{\mathrm{D}t} = \frac{\partial V}{\partial t} + V.\nabla V$$

Thus, when a steady state is reached, the non-stationary term drops, and the advective term

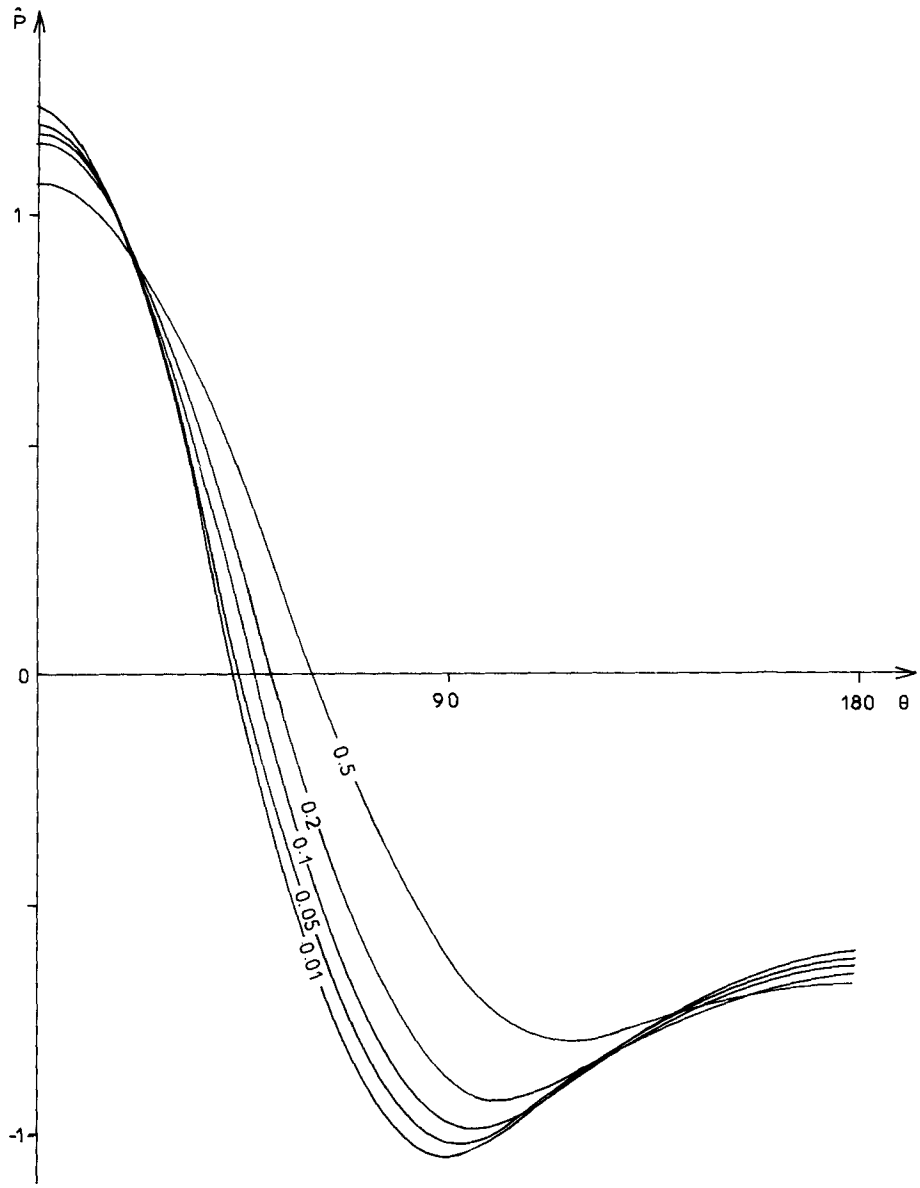

Figure 17. Pressure distribution—influence of the time increment

is no longer dependent on the time increment. With the method of characteristics, we write:

$$\frac{DV}{Dt} = (V - V^*)/\delta t$$

Thus, even when a steady state is reached, the advective terms always remain numerically dependent on t.

Notwithstanding this drawback, the results are acceptable, as we will now see, especially for the velocity field. In the following text, we will only take into consideration our solution for $\delta t = 0{\cdot}1$. It will be compared to other numerical results, and to some experimental data.

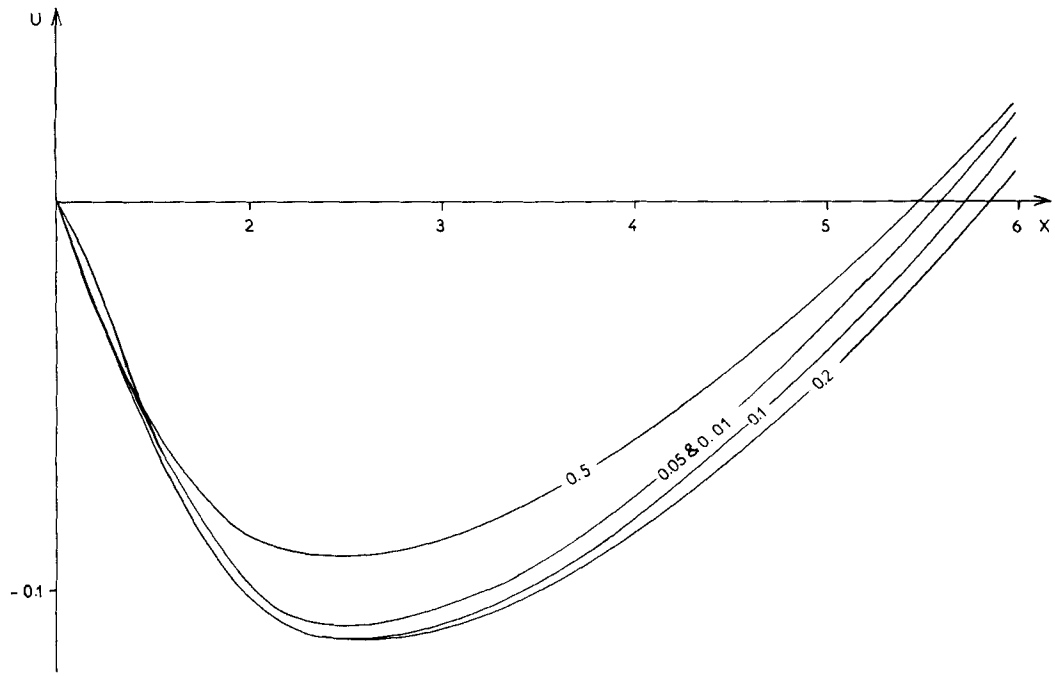

Figure 18. Velocity on the axis behind the cylinder—influence of the time increment

Table II. Drag coefficients for the circular cylinder

δt	C_p	C_ν	C_D
0·5	1·10	0·58	1·68
0·2	1·26	0·56	1·82
0·1	1·16	0·55	1·71
0·05	1·14	0·57	1·71
0·01	1·10	0·58	1·68

6.4. Summary of data available for the comparison

Pressure and shearing stress at the surface of the cylinder have been calculated in particular by Kawaguti[13] and Dennis and Chang.[14] The shearing stress distribution can also be found in a paper by Ta Phuoc Loc.[15] Dimopoulos and Hanratty[16] obtained direct measurements of the shearing stress at the surface of a cylinder for $60 \leq Re \leq 360$. However, to our knowledge, no such measurements were done for $Re = 40$. Thus, we only compare different numerical results for the shearing stress. Pressure measurements where performed by Thom[17] and Grove *et al.*[18] The total drag coefficient was measured by Tritton,[19] and calculated in the numerical works above. Velocity measurements behind a cylinder were conducted by Coutanceau and Bouard,[20] Nishioka and Sato[21] and Taneda.[22]

6.5. Discussion

Figure 19 shows that the different values of $\tau(\theta)$ compare quite well. This good result is particularly encouraging, since it shows that normal derivatives $\partial u_0/\partial n$ can be accurately

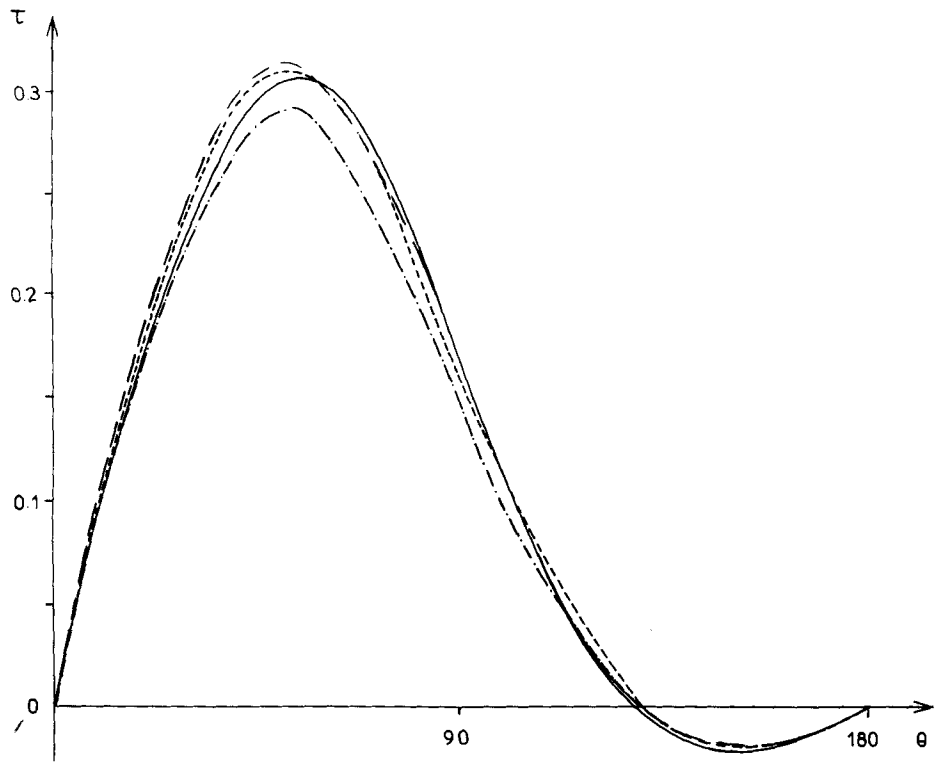

Figure 19. Shearing stress—numerical results: ——— our results; — — — Kawaguti; —·—·— Dennis; - - - - - - - Ta Phouc Loc

determined at the wall, from the velocity field, by deriving the shape function of the boundary elements. Now the shearing stress on a wall is of essential importance in industrial calculations. In Figure 20, our pressure curve is compared to numerical solutions, and experimental points. Agreement is acceptable, though less satisfactory than for the shearing stress. However, it must be noted that some discrepancies were expectable, since the surrounding conditions are different:

(i) Our boundary conditions for velocity (see Figure 18) are compatible with those in Coutanceau's experiment: a moving cylinder in a motionless tank, with a confinement ratio $\lambda = 1/15$. However, our outlet boundary condition for the pressure $p = 0$ could correspond to a discharge in the atmosphere or in a free surface reservoir or to an undisturbed pipe or channel flow, which does not reflect the experimental situation.

(ii) Pressure measurements were done in a channel flow, with $\lambda \leq 0{\cdot}05$. Therefore, a boundary layer along the walls of the channel was present, which is not the case in the present calculations. Moreover, like in Coutanceau's experiments, pressure in the cross-section located at 20 diameters behind the cylinder was certainly not uniform.

(iii) Other quoted numerical calculations were done with the assumption of an infinite medium.

According to Table II, the total drag C_D takes the value 1·7. This value is in very good agreement with other calculated values, and experimental results by Tritton[19] and Nishioka and Sato.[21]

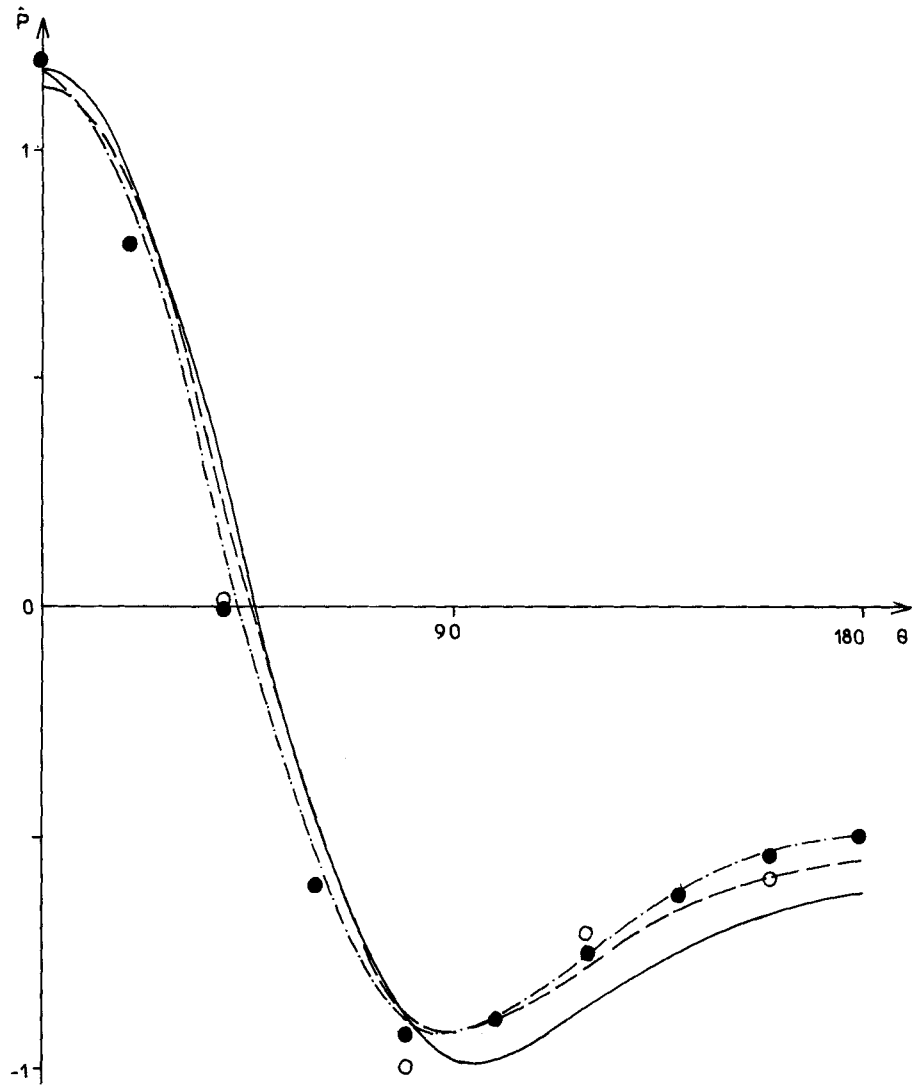

Figure 20. Pressure distribution—numerical results: ——— our results; – – – – Kawaguti; —·—·— Dennis. Experimental results: ● Thom; ○ Grove

To achieve this comparison, Figure 21 displays our result for the u velocity component along the x axis, behind the cylinder, associated with another numerical solution by Kawaguti,[13] and experimental points by Coutanceau and Bouard.[20] The agreement in the first part of the wake between our result and the experimental data is excellent. The position of the separation point is also satisfactory: 128° for an experimental value of 127·2°. A discrepancy appears however, about the length L of the wake $L = 4{\cdot}7$ instead of 4. Since $Re = 40$ is the limiting value for the stability of the wake, it is understandable that the downstream part of the wake is sensitive to wall effect, outlet pressure condition, or local roughness of the grid in this zone. Anyway, this value of 4·7 lies in the range of the various values found in the literature, and reported for instance by Nishioka and Sato;[21]

$$3{\cdot}9 \leq L \leq 4{\cdot}8$$

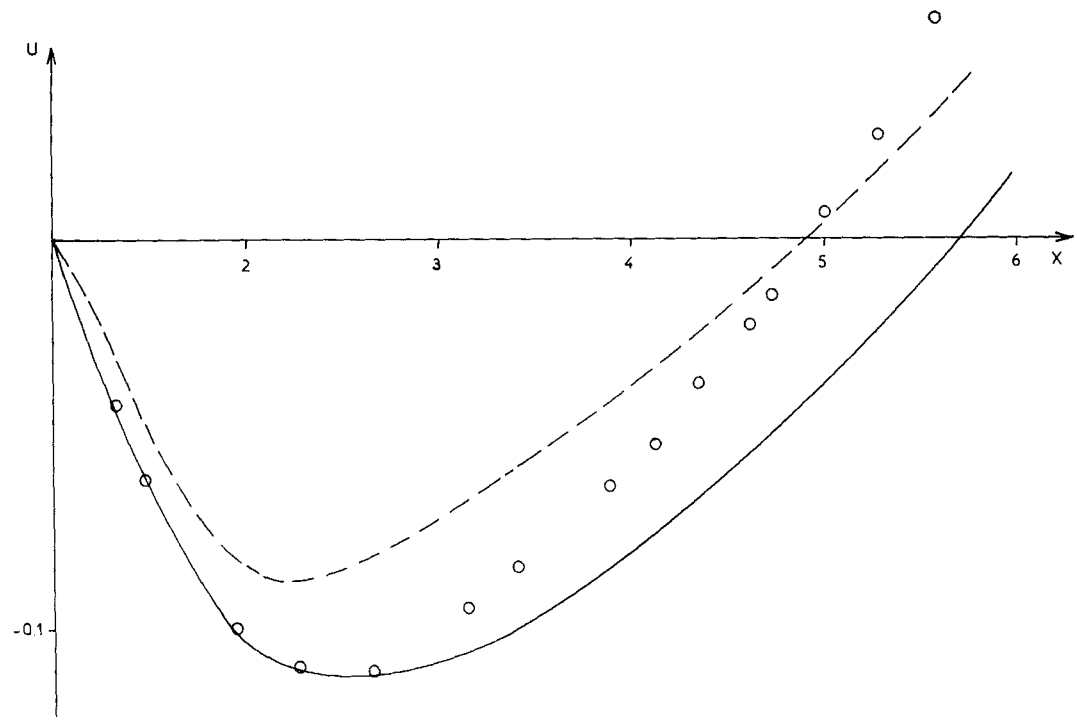

Figure 21. Velocity on the axis behind the cylinder: ——— our results; — — — Kawaguti's numerical results; ○ Coutanceau's experimental results

7. CONCLUSION

Our FE method involving the solution of the Poisson equation (PEFE2) is simple in its principle. It presents no difficulties of coding, except for the curvilinear characteristic. This curvilinear characteristic, however, gives very interesting features to the method: the advection step is explicit, but unconditionally stable. It follows that:

(a) Transient calculations are possible, without theoretical limitation on the time increment. When only the steady solution is needed, stabilization occurs very fast with a large time step, though a short rerun with a smaller time increment is necessary, for the accuracy of the pressure solution.

(b) Since the treatment of non-linearities is explicit, the linear systems to be solved remain symmetric definite positive. Moreover, additional scalar equations with coupling (thermal problems, turbulence models) can be introduced without basic difficulty.

In addition to these theoretical advantages, numerical tests show the encouraging behaviour of our method:

(i) The numerical diffusion due to treatment of advection is very comparable to that occurring with a reliable high order finite difference method.

(ii) The incompressibility condition is very acceptably satisfied.

(iii) The time consumption and core memory requirements are moderate, with regard to some other F.E. methods, such as the 'trace of pressure'.

(iv) Comparison with available experimental data (flow past a cylinder at $Re = 40$) proved to be satisfactory.

Consequently, our method seems to be suitable for more difficult applications, such as for instance calculation of turbulent industrial flows in two or three dimensions.

REFERENCES

1. J. P. Huffenus and D. Khaletzky, 'The Lagrangian approach of advective term treatment and its application to the solution of Navier–Stokes equations', *Int. j. numer. methods fluids*, **1,** 365–387 (1981).
2. J. P. Benque, G. Labadie and B. Ibler, 'A finite element method for the calculation of incompressible viscous flows', *First International Conference on Numerical Methods for non linear equations*, Swansea U.K., September 1980.
3. J. P. Huffenus, 'Calculs d'écoulements en fluide réel', *La Houille Blanche*, N° 6 (1969).
4. P. J. Roache, *Computational Fluid Dynamics*, Hermosa, 1976.
5. J. J. Connor and C. A. Brebbia, *Finite Element Techniques for Fluid Flow*, Newnes–Butterworth, 1978.
6. M. O. Bristeau, R. Glowinski, J. Periaux, P. Perrier, O. Pironeau and G. Poirier, 'Application of optimal control and finite element methods to the calculation of transonic flows and incompressible viscous flows', *IRIA—Rapport de Recherche n° 294*, April 1978.
7. F. Thomasset, *Implementation of Finite Element Methods for Navier–Stokes Equations*, Springer Series in Computational Physics, Springer Verlag (1981).
8. B. Ibler, 'Résolution des équations de Navier–Stokes par une méthode d'éléments finis', *Thèse 3è cycle*, Paris Sud-Centre d'Orsay, January 1981.
9. R. Glowinski, E. Y. Rodin and O. C. Zienkiewicz, *Energy Methods in Finite Element Analysis*, Wiley, 1979, chapter 13.
10. M. Braza, H. Ha Minh, O. Brocard, D. Kalfon and P. Mazet, 'Comparison between three Navier–Stokes solvers', *Proceedings of the IAHR Symposium on Refined Modelling of Flows*, Paris 7, 10 September 1982. Presses de l'Ecole Nationale des Ponts et Chaussées.
11. R. L. Sani, P. M. Gresho, R. L. Lee and D. F. Griffith, 'The cause and cure(?) of the spurious pressures generated by certain FEM solutions of the incompressible Navier–Stokes equations, Part 1, *Int. j. numer. methods fluids*, **1,** 17–43 (1981).
12. M. Fortin, R. Peyret and R. Temam, 'Calcul des écoulements d'un fluide visqueux incompressible', *J. Mecanique*, **10,** 357 (1971).
13. M. Kawaguti, 'Numerical solution of the Navier–Stokes equations for the flow around a circular cylinder at Reynolds number 40', *J. Phys. Soc. Japan*, **8,** 747 (1953).
14. S. C. R. Dennis and G. Z. Chang, 'Numerical solutions for steady flow past a circular cylinder at Reynolds numbers up to 100', *J. Fluid Mech.*, **42,** 471 (1970).
15. Ta Phuoc Loc, 'Etude numérique de l'écoulement d'un fluide visqueux incompressible autour d'un cylindre fixe ou en rotation; Effet Magnus', *J. Méc.*, **14,** 109 (1975).
16. H. G. Dimopoulos and T. J. Hanratty, 'Velocity gradients at the wall for flow around a cylinder for Reynolds numbers between 60 and 360', *J. Fluid Mech.*, **33** (Part 2) (1968).
17. A. Thom, 'The flow past circular cylinders at low speeds', *Proc. Roy. Soc.*, **A141,** 651 (1933).
18. A. S. Grove, F. H. Shair, E. E. Peterson and A. Acrivos, 'An experimental investigation of the steady separated flow past a circular cylinder', *J. Fluid Mech.*, **19,** 60 (1964).
19. D. J. Tritton, 'Experiments on the flow past a circular cylinder at moderate Reynolds numbers', *J. Fluid Mech.*, **37,** 95 (1959).
20. M. Coutanceau and R. Bouard, 'Experimental determination of the main features of the viscous flow in the wake of a circular cylinder in uniform translation, Part 1—Steady flow', *J. Fluid Mech.*, **79,** 231 (1977).
21. M. Nishioka and H. Sato, 'Measurements of velocity distributions in the wake of a circular cylinder at low Reynolds numbers', *J. Fluid Mech.*, **65,** 97 (1974).
22. S. Taneda, 'Experimental investigation of the wakes behind cylinders and plates at low Reynolds numbers'. *J. Phys. Soc. Japan*, **11,** 302 (1956).